New Journal of Physics
The open-access journal for physics

Searching for Si-based spintronics by first principles calculations

Mahboubeh Hortamani[1,2], Leonid Sandratskii[1], Peter Kratzer[2,3] and Ingrid Mertig[1,4]

[1] Max-Planck-Institut für Mikrostrukturphysik, D-06120 Halle, Germany
[2] Fritz-Haber-Institut der Max-Planck-Gesellschaft, Faradayweg 4-6, D-14195 Berlin, Germany
[3] Fachbereich Physik, Universität Duisburg-Essen, D-47048 Duisburg, Germany
[4] Fachbereich Physik, Martin-Luther-Universität Halle-Wittenberg, D-06099 Halle, Germany
E-mail: hortamani@mpi-halle.mpg.de

New Journal of Physics **11** (2009) 125009 (23pp)
Received 7 July 2009
Published 11 December 2009
Online at http://www.njp.org/
doi:10.1088/1367-2630/11/12/125009

Abstract. Density functional theory (DFT) calculations are used to study the epitaxial growth and the magnetic properties of thin films of MnSi on the Si(001) surface. For adsorption of a single Mn atom, we find that binding at the subsurface site below the Si surface dimers is the most stable adsorption site. There is an energy barrier of only 0.3 eV for adsorbed Mn to go subsurface, and an energy barrier of 1.3 eV for penetration to deeper layers. From the calculated potential-energy surface for the Mn adatom we conclude that the most stable site on the surface corresponds to the hollow site where Mn is placed between two Si surface dimers. Despite Si(001) geometrically being an anisotropic surface, the on-surface diffusion for both directions along and perpendicular to the Si dimer rows has almost the same diffusion barrier of 0.65 eV. For coverage above 1 ML, the lowest energy structure is a pure Mn subsurface layer, capped by a layer of Si adatoms. We conclude that the Mn-silicide films stabilize in an epitaxially CsCl-like (B2) crystal structure. Such MnSi films are found to have sizable magnetic moments at the Mn atoms near the surface and interface, and ferromagnetic coupling of the Mn clarify within the layers. Layer-resolved electronic densities-of-states are presented that show a high degree of spin polarization at the Fermi level, up to 30 and 50% for films with one or two MnSi films, respectively.

In order to clarify the stability of ferromagnetism at finite temperatures we estimate the Curie temperature (T_c) of MnSi films using a multiple-sublattice Heisenberg model with first- and second-nearest neighbor interactions

determined from DFT calculations for various collinear spin configurations. The Curie temperature is calculated both in the mean-field approximation (MFA) and in the random-phase approximation (RPA). In the latter case, we find a weak logarithmic dependence of T_c on the magnetic anisotropy parameter, which was calculated to be 0.4 meV. Large Curie temperatures of above 200 K for a monolayer MnSi film, and above 300 K for a 2 ML MnSi film are obtained within the RPA, and even higher values in MFA.

Complementary calculations are performed for non-collinear spin structures to study the limitations of the mapping of the system onto a Heisenberg model. We demonstrate that biquadratic interatomic exchange interactions and longitudinal fluctuations of atomic moments give important contributions to the energetics of the system.

Contents

1. Introduction

One of the main goals of spintronics is to combine semiconductor technology with magnetic materials, aiming at the injection of a spin-polarized current from a ferromagnet into a semiconductor. From a general point of view, this ferromagnetic electrode could consist of a magnetic transition metal, or of a magnetic silicide (either metallic or semiconducting), or of a dilute magnetic semiconductor. To identify candidates that are suitable to be employed for spin injection, the material should fulfil the following criteria: (i) structural stability as an epitaxial film on the substrate, (ii) sharp and structurally well-defined interface with the substrate, (iii) high temperature of the magnetic ordering and high degree of spin polarization at the interface.

Heterostructures made from a ferromagnetic material and silicon can be achieved essentially in two ways, either by depositing a structurally well-defined thin film of a ferromagnetic metal on silicon, or by turning silicon into a dilute magnetic semiconductor. It has been shown theoretically that ultrathin films of manganese-silicides on silicon are of relevance as a possible material system for building spintronics devices with silicon technology. These films are predicted to display ferromagnetic (FM) behavior, a considerable degree of spin polarization of carriers at the MnSi/Si(001) interface and high magnetic transition temperature [1]–[4]. These properties make heterostructures of these types of materials on silicon promising for efficient spin injection. The possibility to grow strongly doped Mn:Si,

which could possibly be ferromagnetic has also been explored theoretically [5]–[8]. Despite some progress with dilute magnetic semiconductors, experimentally a ferromagnetic diluted magnetic semiconductor with a Curie temperature above room temperature has not been achieved up to now.

Recently, some experimental progress has been made in growing well-defined MnSi nanostructures, both as small two-dimensional (2D) islands [9] and in the form of atomic nanowires [10]. For fabricating the above-mentioned structures, it is desirable to have a good theoretical understanding of the adsorption, diffusion and nucleation of Mn on the silicon surface as well as of the thermodynamic stability of the FM phase of MnSi.

This paper is organized as follows: firstly, we investigate the behavior of single Mn adatoms on Si(001). To identify the elementary growth processes that determine the interface quality, we need information about the diffusion pathways of Mn on Si and their energy barriers. Subsequently, we discuss the formation of ordered films, their stability, and the magnetic and electronic properties of multilayer MnSi films. To study magnetic properties of the film at finite temperature, we map this system onto a Heisenberg Hamiltonian. After obtaining the size of exchange interactions from density functional theory (DFT) calculations, we estimate the Curie temperature of the MnSi films on the Si(001) surface using either the mean-field (MFA) or the random-phase approximation (RPA). In this context, it is advisable also to discuss the limitations of the mapping of the magnetic MnSi interactions onto a Heisenberg model. Two types of such limitations are considered: fluctuations of the direction of magnetic moment (transversal fluctuations) and fluctuations of the magnitude of the magnetic moment (longitudinal fluctuations). Finally, we discuss the validity of the Heisenberg model for this system.

2. Methods and calculational details

We employ DFT to determine the atomic structure, the relative stability, and the magnetic properties at zero temperature of numerous structures that occur during adsorption, bulk incorporation and thin film growth of Mn on Si(001). We use the *full-potential augmented plane-wave plus local-orbital* method [11], which is implemented in WIEN2k computer package [12]. The generalized gradient approximation (GGA-PBE96) [13] for the exchange-correlation potential is employed, since it has been demonstrated [14] and confirmed by our own calculations that it gives a much better description for bulk Mn than the local-spin-density approximation (LSDA) [15].

A slab geometry is used to model the Si(001) surface consisting of eight (or, in some cases, ten) layers of Si atoms. Mn adatoms are placed on top and bottom surfaces of the slab to preserve the inversion symmetry of the supercell. We define a monolayer (ML) coverage of Mn by having a space-filling arrangement of two Mn adatoms per (1×1) unit cell of the Si(001) surface. For a single Mn coverages, the calculations were performed in a $p(2 \times 2)$ unit cell using a surface reconstruction with alternatingly buckled Si dimers. The slabs are separated by a vacuum region of 16.4 Å. The Brillouin zone sampling in this case is done by a set of 10 **k**-points in the irreducible part of the Brillouin zone, derived from a $10 \times 10 \times 1$ **k**-point mesh. The muffin-tin sphere radius is set to 1.11 Å for both Mn and Si, and the cut-off energy for the plane-wave expansion in the interstitial region is 13.8 Ry. Such rather low cut-off energy is appropriate because of using additional local orbitals as basis functions [11]. All Mn and Si atoms except for the two central-layer Si atoms were relaxed until all atomic forces are smaller

than 0.03 eV Å^{-1}. The numerical accuracy of the present calculations has been checked for the clean Si(001) surface using a higher cut-off energy and number of **k**-points. It was found that the surface energy is converged within 0.01 eV per (1×1) cell. Moreover, calculations for MnSi with different choice of the muffin-tin radii showed that changes are less than 0.02 eV per (1×1) cell [16].

Although DFT is the best approach to describe the ground-state properties of systems, the description of finite temperature properties, such as the Curie temperature, is not straightforward. A standard and convenient way to estimate the Curie temperature of an itinerant-electron system is to map the system onto an effective Heisenberg Hamiltonian of interacting atomic magnetic moments [17][5].

For a multisublattice crystalline system the Heisenberg Hamiltonian can be written in the form

$$H = -\sum_{\mathbf{R},\mathbf{R}',\mu,\nu} J^{\mu\nu}_{\mathbf{R}\mathbf{R}'} \mathbf{e}^{\mu}_{\mathbf{R}} \cdot \mathbf{e}^{\nu}_{\mathbf{R}'} \tag{1}$$

where the parameters $J^{\mu\nu}_{\mathbf{R}\mathbf{R}'}$ describe the exchange interaction between two atoms; $\mathbf{R}$, $\mathbf{R}'$ are unit cell indices; μ ν are sublattice (basis site) indices; and $\mathbf{e}^{\mu}_{\mathbf{R}}$ is the unit vector pointing in the direction of the magnetic moment at site (μ, R). Because of the crystal periodicity $J^{\mu\nu}_{\mathbf{R}\mathbf{R}'} = J^{\mu\nu}_{\mathbf{R}-\mathbf{R}',0}$. The on-site exchange parameters in equation (1) are equal to zero: $J^{\mu\mu}_{\mathbf{R}\mathbf{R}} = 0$. The vector $\mathbf{e}$ is assumed to take arbitrary directions that corresponds to the classical treatment of an atomic magnetic moments. This is a plausible description of a weak itinerant-electron magnet.

The procedure of the mapping of an itinerant electron system on the Heisenberg Hamiltonian consists in the determination of the interatomic exchange parameters $J^{\mu\nu}_{\mathbf{R}\mathbf{R}'}$ on the basis of the first-principles calculations. We begin with a simpler scheme and determine the Heisenberg exchange parameters on the basis of the calculated total energies of a number of collinear magnetic configurations obtained by the reversal of the directions of some of the atomic moments. This calculations require, however, the use of large magnetic supercells. Since the change of the interspin angles obtained by reversal of the atomic moments is as large as 180°, the corresponding states of the system have low statistical weight in the statistical mechanics of the thermal magnetic disordering.

It is worth noting that the Fermi level determined with the use of the slab geometry will deviate slightly from the Fermi level determined within the treatment of the substrate as a half-infinite crystal. This difference does not, however, influence noticeably physical properties discussed in the paper. In particular, the values of the exchange parameters are very robust in this respect since they are determined by the difference of the total energies of various spin configurations of the magnetic film that leads to the cancelation of the small inaccuracies related to the determination of the Fermi level.

The obtained exchange parameters are used to estimate the Curie temperature employing two approaches: the MFA and the RPA. For 3D solids the MFA is expected to overestimate the value of the Curie temperature, whereas the RPA is expected to underestimate T_c [19]. The RPA accounts for spin-wave excitations and is supposed to give a better estimate of the Curie temperature than the MFA. For the two-dimensional systems treated in RPA there is

[5] The concept of using a model Hamiltonian in which parameters are determined by DFT calculations is a standard approach which has been used before; for example, in the lattice-gas Hamiltonian approach see [18].

an additional complication related to the Mermin–Wagner theorem [20]. This issue has been discussed in detail in our previous paper [3].

The main physical quantity in the MFA is the effective exchange field experienced by a given magnetic moment from all other magnetic atoms. The statistical mechanics in the MFA is the statistical mechanics of individual atomic spins in an effective exchange field originating from the interaction with the environment. The long wavelength fluctuations are neglected in the MFA and the conditions of the Mermin–Wagner theorem are violated. On the other hand, the RPA deals with the wavevector-dependent spin-wave excitations and, in agreement with the Mermin–Wagner theorem, gives for a 2D isotropic ferromagnet a zero value of the Curie temperature. Thus, for the 2D systems the use of the RPA is preferable. The MFA value of the Curie temperature can still be considered as a useful characteristic of the exchange interactions in the system. Therefore we present both MFA and RPA estimations of the Curie temperature.

The MFA estimation of the Curie temperature of a multi-sublattice system can be obtained by solving the system of coupled equations [21]–[23]

$$\langle e_\mu^z \rangle = \frac{2}{3k_{\mathrm{B}}T_{\mathrm{c}}} \sum_\nu J_0^{\mu\nu} \langle e_\nu^z \rangle, \tag{2}$$

where $J_0^{\mu\nu} \equiv \sum_{\mathbf{R}} J_{0\mathbf{R}}^{\mu\nu}$. Equation (2) can be rewritten in the form of an eigenvalue problem

$$(\Theta - \mathbf{T_c I})\mathbf{S} = 0, \tag{3}$$

where $\Theta_{\mu\nu} = (2/3k_{\mathrm{B}})J_0^{\mu\nu}$, $\mathbf{I}$ is a unit matrix and $\mathbf{S}$ is the vector set of $\langle e_\nu^z \rangle$. The largest eigenvalue of the matrix gives the value of $T_{\mathrm{c}}^{\mathrm{MFA}}$ [21]–[23].

The RPA approach to the calculation of the Curie temperature of multiple-sublattice systems has been discussed in [24]. The derivation of the RPA method starts with the consideration of the Heisenberg Hamiltonian of quantum spins. Rusz *et al* [24] arrive at the following formula

$$k_{\mathrm{B}}T_{\mathrm{c}} = \frac{2}{3\langle \tilde{s}_\mu^z \rangle} \frac{S_\mu + 1}{S_\mu} \left\{ \frac{1}{\Omega} \int \mathrm{d}\mathbf{q} \left[N^{-1}(\mathbf{q})_{\mu\mu} \right] \right\}^{-1}, \tag{4}$$

where k_{B} is the Boltzmann constant and $\tilde{s}_{i\mu}^z = S_{i\mu}^z / S_\mu$. Here, $S_{i\mu}^z$ is the z-component of the spin of the site (μ, i), S_μ is the value of the spin of the atoms of type μ. The average value of $\tilde{s}_{i\mu}^z$ does not depend on i. $[N^{-1}(\mathbf{q})_{\mu\mu}]$ in equation (4) is the diagonal element of the matrix inverse to matrix N defined by

$$N_{\mu\nu} = \delta_{\mu\nu} \left(\Delta + \sum_\eta J_{\mu\eta}(\mathbf{0}) \langle s_\eta^z \rangle \right) - \langle s_\mu^z \rangle J_{\mu\nu}(\mathbf{q}). \tag{5}$$

Here, Δ gives the magnetic anisotropy energy (MAE). The value of Δ can be estimated on the basis of the first-principles calculations with the spin–orbit coupling taken into account. It is given by the energy difference of the FM states with different directions of the magnetic moments.

At the next stage, to get deeper insight into the magnetic interactions we extend the calculations to non-collinear magnetic structures. The energies of spiral magnetic configurations with different wave vectors and different amplitudes of deviations from the ground-state structure allow us to account for long-range exchange interactions and to discuss the limitations of the Heisenberg model. The DFT calculations for the non-collinear magnetic configurations

are performed using the augmented spherical wave (ASW) method [25, 26]. We use the frozen-magnon approach to determine the exchange parameters on the basis of DFT calculations for spin spiral structures. This method allows the use of the magnetic configurations with arbitrary angles between atomic magnetic moments. Therefore, the dependence of the exchange parameters on the choice of the magnetic configurations can be studied.

The technique for the determination of the Heisenberg exchange parameters for a complex lattice was recently discussed in detail in [27]. Here, we give a brief outline of the method. The frozen magnon of the νth sublattice characterized by wave vector $\mathbf{q}$ is defined by the expression

$$\mathbf{e}_{\mathbf{R}}^{\nu} = [\sin\theta^{\nu}\cos(\phi^{\nu}(\mathbf{q}) + \mathbf{qR}), \sin\theta^{\nu}\sin(\phi^{\nu}(\mathbf{q}) + \mathbf{qR}), \cos\theta^{\nu}], \tag{6}$$

where θ^{ν} is the polar angle of the frozen magnon and ϕ^{ν} is the initial phase angle of the sublattice that can be different for different $\mathbf{q}$.

The evaluation of the exchange parameters involves several steps. To find the interaction parameters between the spins of the same sublattice ν, we substitute equation (6) into equation (1), taking a nonzero value of $\theta^{\nu} = \theta$. The polar angles of other sublattices are set to zero. The Heisenberg energy of such structures takes the form

$$E^{\nu\nu}(\theta, \mathbf{q}) = E_0^{\nu\nu}(\theta) - \sin^2(\theta) J^{\nu\nu}(\mathbf{q}) \tag{7}$$

where $E_0^{\nu\nu}(\theta)$ does not depend on $\mathbf{q}$. Performing *ab initio* calculation of $E^{\nu\nu}(\theta, \mathbf{q})$ for a regular $\mathbf{q}$ mesh and making back Fourier transformation

$$J_{\mathbf{0R}}^{\nu\nu} = \frac{1}{N}\sum_{\mathbf{q}} J^{\nu\nu}(\mathbf{q})\exp(-\mathbf{iqR}), \tag{8}$$

we obtain the intrasublattice exchange parameters. Here, N is the number of the points in the $\mathbf{q}$ mesh.

To find the exchange parameters for atoms belonging to two different sublattices ν and μ, we take the nonzero value of the polar angle for these two sublattices: $\theta^{\nu} = \theta^{\mu} = \theta \neq 0$. The Heisenberg energy of such magnetic structure after some algebra can be represented in the form

$$\begin{aligned} E^{\mu\nu}(\theta, \mathbf{q}, \Delta^{\mu\nu}(\mathbf{q})) = {} & E_0^{\mu\nu}(\theta) - \sin^2(\theta)[J^{\nu\nu}(\mathbf{q}) + J^{\mu\mu}(\mathbf{q})] + \exp(-\mathrm{i}\Delta\phi^{\mu\nu}(\mathbf{q}))J^{\mu\nu}(\mathbf{q}) \\ & + \exp(-\mathrm{i}\Delta\phi^{\mu\nu}(\mathbf{q}))J^{\mu\nu}(-\mathbf{q}), \end{aligned} \tag{9}$$

where $E_0^{\nu\mu}(\theta)$ is a $\mathbf{q}$-independent contribution to the energy. The single sublattice terms $J^{\nu\nu}$ and $J^{\mu\mu}$ are known from the first step. Again, to find the inter sublattice exchange parameters, one needs to perform a back Fourier transformation of $J^{\mu\nu}(\mathbf{q})$.

Strictly speaking, the system understudy is *not* a system of localized magnetic moments, as there is strong hybridization between Mn atoms as well as between Mn and Si atoms. Therefore limitations of the standard Heisenberg picture (dealing with well-defined atomic magnetic moments) are to be expected in the case of MnSi films [28]. To study the validity of the Heisenberg model we consider two types of limitations of the model. Firstly, keeping the assumption of the Heisenberg model that only the directions of the atomic moments are relevant degrees of freedom, we investigate the role of a higher order bi-quadratic exchange interaction between atomic spins. Secondly, by restricting the consideration to the orientational degrees of freedom, the Heisenberg model takes into account the transversal fluctuations of

the atomic moments and neglects the longitudinal fluctuations of the moments. However, in itinerant electron systems the atomic moments can fluctuate not only in direction but also in magnitude. To study these longitudinal fluctuations we use the so-called fixed-spin-moment method consisting in the constrained minimization of the total energy functional [29]. The desired value of the atomic moment m is stabilized by an effective constraining magnetic field that depends on m and is determined self-consistently.

3. Results and discussion

3.1. Initial adsorption and surface diffusion pathway

The first step to understand the growth process is having information about the binding sites, diffusion pathways and energy barriers for the migration of an adsorbed atom on the surface. This can be done by mapping the energy of the system while the adsorbate is sitting in different positions inside the surface unit cell. This map is called the potential energy surface (PES). In order to characterize the binding sites and study the preferential migration paths of a Mn atom on silicon substrates, we present a comprehensive study of the adsorption and diffusion of a Mn adatom on the (2×2) reconstruction of Si(001), via DFT calculations. The PES is defined by relaxing both the height (Z_{Mn}) of the Mn adatom from far above the surface (for a set of fixed lateral coordinates, X_{Mn}, Y_{Mn}, of the Mn atom), as well as all coordinates of the substrate atoms. In order to quantitatively discuss the PES of a Mn adatom, we carried out calculations of the adsorption energy using

$$E_{\mathrm{ad}}(X_{\mathrm{Mn}}, Y_{\mathrm{Mn}}) = \min_{\mathbf{R}} \min_{Z_{\mathrm{Mn}}} E^{\mathrm{tot}}_{\mathrm{system}}(\mathbf{R}, \mathbf{R}_{\mathrm{Mn}}) - E^{\mathrm{slab}} - E^{\mathrm{Mn}}.$$

Here $\mathbf{R}$ denotes the position of the substrate atoms, and E^{Mn} is the energy of a free Mn atom in its ground state. The total energy of the clean slab, E^{slab}, is obtained by a separate calculation for the clean Si(001) surface. With this definition, E_{ad} reflects the adsorption energy of a Mn adatom on Si(001). Local minima in the PES constitute (meta-)stable binding positions of the adatom, and saddle points correspond to transition states for adatom diffusion. Energy barriers for diffusion are calculated as the energy differences between the transition state energy and the energy at the minimum of the PES. This describes the initial state of the growth process.

For a single Mn atom adsorption, we find that binding at the subsurface site (below the Si surface dimers) is about 0.9 eV stronger than on-surface adsorption. This has been observed experimentally [9]. The adsorption energy at the high-symmetry site between two dimers in the same row on the surface (hollow site) is about 2.9 eV.

In the context of the epitaxial growth of Mn-doped Si, incorporation of Mn at substitutional positions at the surface is particularly important. On the one hand, this process is likely to trigger silicide formation. On the other hand, it has long been known that substitutional Mn atoms in bulk Si act as acceptors [30] with a large local magnetic moment, and hence one could speculate that Si could be turned into a magnetic semiconductor if substitutional Mn incorporation with a high concentration could be achieved. We therefore studied the energetics of Mn replacing a Si atom of the Si surface dimer. If we take the chemical potential of bulk Si as energy reference, substitutional adsorption is energetically less favorable than adsorption into the subsurface interstitial site, by 0.94 eV.

To obtain a clearer picture of the diffusion pathways *on* the Si(001) surface, the 2D PES is drawn in figure 1. There are two types of local minima in the PES: one in the hollow site (marked

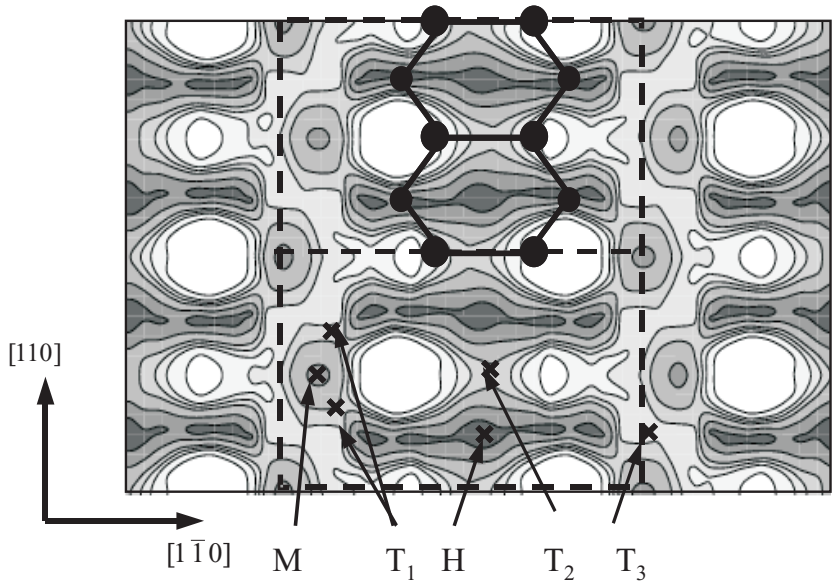

Figure 1. The PES of a Mn atom on Si(001). The diffusion barriers for hopping between on-surface minima H are 0.65 eV. Diffusion along [$\bar{1}$10] (between Si dimer rows) occurs via transition state T_3. Diffusion along [1 1 0] proceeds either through transition state T_2 or through transition state T_1 and intermediate M. The darker areas show low-potential sites (binding sites) and the brighter parts belong to the high-energy positions.

H in figure 1). The other is between two dimers in adjacent rows (marked M in figure 1). The Mn atom binds most strongly at the hollow site.

For on-surface diffusion between two hollow sites, there exist three low-energy pathways, two of them along the Si dimer rows: one where the adatom passes the (still intact) Si dimer through saddle point T_2, and another pathway via the minimum M, passing twice through symmetry-equivalent saddle points T_1. For the first diffusion pathway, the energy barrier is about 0.65 eV (see figure 1), while it is slightly lower (0.55 eV) for the second pathway (see figure 1, lower right panel). The third diffusion pathway is from one hollow site to the next one, perpendicular to the dimer row. In the latter pathway the Mn adatom needs to overcome a barrier of 0.65 eV at T_3 (see figure 1, lower left panel).

Although the surface of Si(001) is structurally anisotropic, surprisingly we find out that the Mn atom diffuses almost isotropically along and perpendicular to the dimer rows (see curves in figure 2).

We consider how the Mn adatom diffuses into the second layer site, i.e. how it reaches the interstitial site from the hollow site (which is the energetically the most stable binding site on the surface). We plot the PES for a Mn atom in a ($1\bar{1}0$) plane perpendicular to the surface, which intersects both the hollow and the interstitial sites. We fix the Mn atom at a set of positions in this plane, and relax the substrate Si atoms in each case. It is seen that for the most favorable pathway the Mn adatom first moves slightly upward away from the hollow site. Thereby, the surface Si dimer is elongated, thus giving room for the Mn atom to find its way to the subsurface interstitial site. The energy barrier of only 0.3 eV must be overcome for adsorbed Mn to go subsurface, and an energy barrier of 1.2 eV for the reverse process. The energy barrier between hollow and

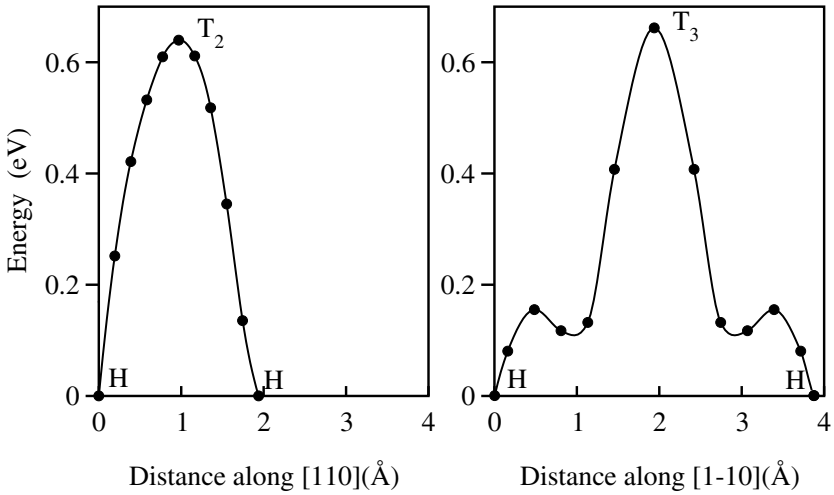

Figure 2. The Mn diffusion is almost isotropic as long as only on-surface hopping processes are considered.

interstitial site is shown in figure 3. For more information about the subsurface pathway and the PES we refer to our previous paper [2].

Now to address the question of whether or not the Mn atom diffuses to deeper layers and even into Si bulk, we performed calculations for the incorporation a Mn atom on third-layer interstitial sites. Our results indicate that the third-layer interstitial site is energetically less favorable than the second-layer interstitial site. There are high-energy barriers for diffusion of Mn into deeper layers. To reach the third-layer site, Mn must overcome an energy barrier of 1.3 eV, measured from the second-layer interstitial site (figure 3). As a result, due to this energy barrier, Mn atoms, even after penetrating to the subsurface site, prefer to diffuse mainly through the on-surface (H) site, rather than through a bulk diffusion mechanism.

We conclude that the Si(001) surface is well suited for growing Mn since Mn incorporation is most favorable in the subsurface position, but becomes less favorable with increasing depth below the surface. Together with the low solubility of Mn in Si bulk [31], this leads to the tendency of Mn atoms to stay near the surface even if deposited at finite substrate temperatures.

3.2. Epitaxial growth of MnSi on Si(001)

There are a few experimental results on the growth of Mn on Si(001) [32]. They are all agreed on the point that a pure Mn film cannot be grown on this surface, but hetero-structures consisting of Mn–Si compounds are observed. Lippitz *et al* [32] observed a flat island of manganese monosilicide alloy. The natural crystal structure of bulk MnSi is the B20 structure. Since, however, the B20 lattice has strong lattice mismatch with the Si(001) substrate, a CsCl crystal structure (B2) has been suggested which could be grown epitaxially on Si(001) [1]. The epitaxial thin films of materials sometimes grow in a crystal structure, which is different from their bulk structure (pseudomorphical growth). This is explained by the presence of strain and/or interface and surface energy contributions. For example, the epitaxial growth of FeSi and CoSi has been observed in B2 structure on Si(111) under non-equilibrium conditions with molecular beam epitaxy [33].

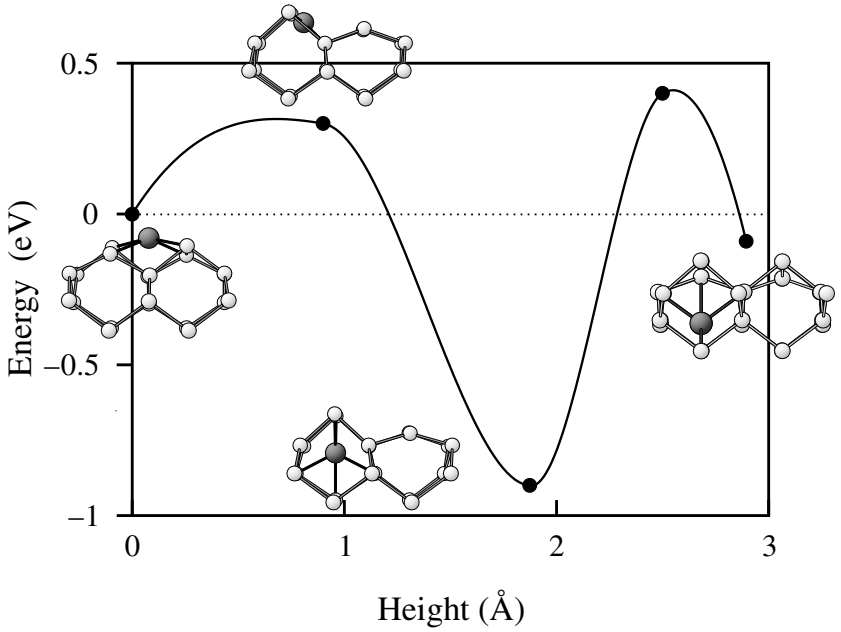

Figure 3. A Mn atom in the hollow site (left structure) has to overcome an energy barrier of only 0.3 eV for to go subsurface (lower structure), and an energy barrier of 1.2 eV for the reverse process. To reach the third-layer site (right structure), Mn must overcome an energy barrier of 1.3 eV, measured from the subsurface site. All structures in this figure are drawn in the yz-plane, i.e. the Si surface dimers of Si(001) are perpendicular to the paper sheet.

We define the film of one or more layers of MnSi alloy by having a space-filling arrangement of alternating layers of two Mn and two Si per layer per (1×1) surface unit cell of the Si(001) surface. It is appropriate to use a (1×1) unit cell to reduce calculational cost. The use of such a small unit cell has no influence on analyzing the properties of multilayer films since the Si dimer reconstruction is lifted already after deposition of 1/2 ML of Mn [2]. It is convenient for the quantitative discussion to consider the stability of the film in terms of its formation energy. This is defined as

$$E_{\text{form}} = (E_{\text{total}} - N_{\text{Si}}\mu_{\text{Si}} - N_{\text{Mn}}\mu_{\text{Mn}})/2 - E^{\text{surf}}_{\text{Si(001)}},$$

where E_{total}, N and μ_k refer to the total energy per (1×1) supercell, the number of atoms in the (1×1) cell, and the chemical potential of the atomic species k. We assume formation of the films from the chemical elements Mn and Si, i.e. the chemical potentials are determined by the cohesive energies of bulk Mn and bulk Si. For bulk Mn, we use the cohesive energy of the ground state α-Mn, by applying a correction of $-0.07\,\text{eV}\,\text{Mn}^{-1}$ [34] to our calculated cohesive energy of γ-Mn (fcc structure). $E^{\text{surf}}_{\text{Si(001)}}$ represents the surface energy of the clean, reconstructed Si(001) surface, being 1.25 eV per (1×1) surface unit cell in our calculations.

In figure 4, we plot the formation energy of a film of MnSi alloy versus the film thickness and compare it with pure a Mn film terminated by a Si layer. The formation energy for Mn overlayers increases monotonously with the Mn coverage and is higher than that of the Si(001) surface (reference energy). We therefore conclude that the growth of pure Mn on the Si(001) surface is energetically rather unfavorable and we turn to Mn–Si compound structures. In

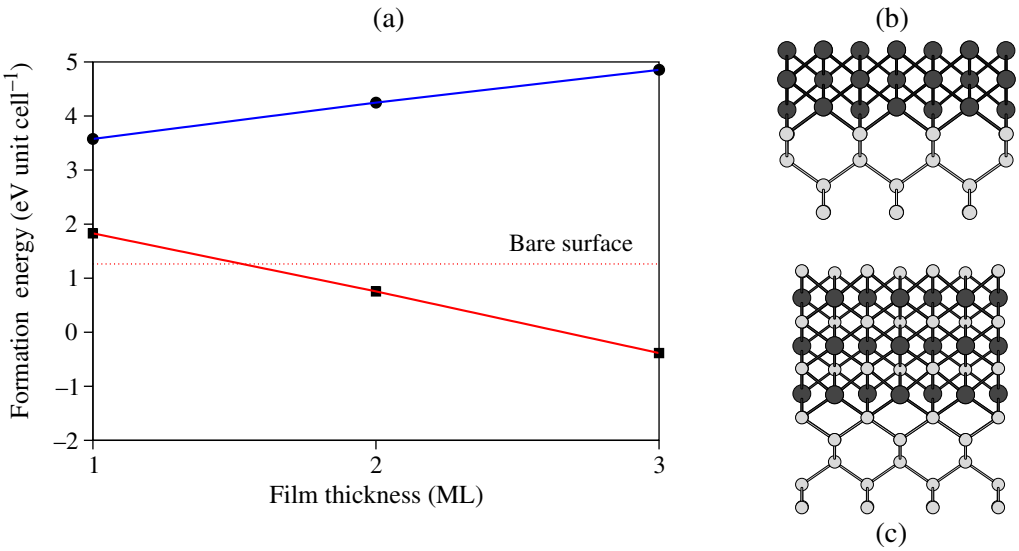

Figure 4. (a) Formation energy of MnSi films with B2 crystal structure on Si(001) (red line) and of pure Mn films capped Si (blue line). As a reference the surface energy of the clean Si(001) $p(2 \times 2)$ reconstructed surface is shown as dotted line. (b) and (c) are ball-stick model for pure Mn film and MnSi sandwich layer, respectively. Black (white) circles are Mn (Si) atoms.

contrast to the pure Mn, the formation energy of the MnSi alloy film decreases with increasing film thickness. For a film thickness of two ML or greater the MnSi alloy is more stable than the clean Si surface. These findings can be rationalized by the fact that Mn–Si bonds are stronger than the average of Mn–Mn and Si–Si bonds; hence the system tends to maximize the number of Mn–Si bonds. In the alternating Mn–Si layers (sandwich of Mn and Si layers), the local coordination of a Mn atom is similar to the bonding in the cesium chloride (B2) crystal structure, i.e. each Mn atom has eight Si neighbors. However, due to epitaxial strain, the local environment of a Mn atom does not have cubic symmetry, but is slightly distorted, and the Mn–Si bond lengths vary by several per cent within the film, being shortest in its interior and longer near the surface and interface.

As a result, the theoretical investigation shows that formation of a well-ordered film of MnSi alloy in B2 crystal structure on Si(001) is possible.

3.3. Magnetic properties at zero and finite temperature

In the previous section, we showed that the films with B2 crystal lattice have layered magnetic structures. The properties of ultrathin films are sensitive to the film thickness. The interlayer magnetic coupling changes from FM to antiferromagnetic (AFM) with increasing film thickness from 2 to 3 ML. A similar effect has been found at the coverage of 1 ML: the transition of the intralayer magnetic structure from AFM to FM when the Mn layer is capped by a Si layer. This effect is caused by Mn–Si hybridization.

The role of Mn–Si hybridization in the formation of the magnetic ground state can be understood on the basis of the nonmagnetic local density of states (LDOS). According to the Stoner criterion [35], the large peak of the density of states (DOS) at the Fermi energy indicates

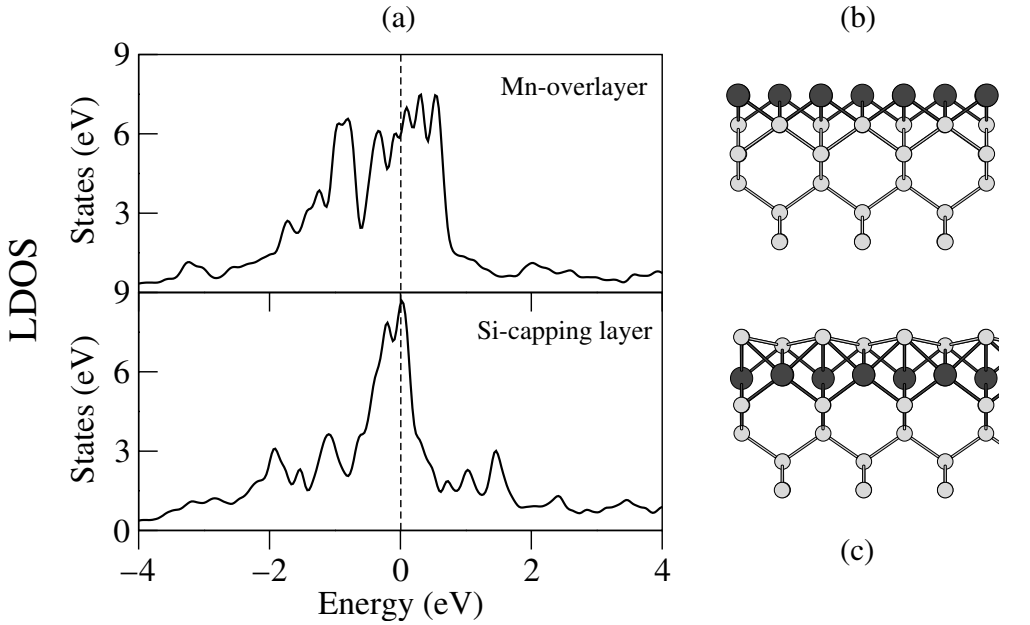

Figure 5. (a) LDOS of a (hypothetical) non-magnetic configuration, projected onto the Mn atom for the structure with one uncapped Mn layer (upper panel), and the Mn layer capped with one Si layer (lower panel). The energy zero is at the Fermi level. The high values of the LDOS at the Fermi level demonstrate that the non-magnetic structures are unstable according to the Stoner criterion. (b) and (c) are ball-and-stick models for the Mn overlayer and the Si capping layer, respectively. Black (white) circles are Mn (Si) atoms.

that the system is unstable and tends to develop magnetic moments. Figure 5 shows that the LDOS at the Fermi level is substantially higher for the Si capped layer. Therefore, the instability of the capped film with respect to the formation of the FM structure is larger than for the uncapped film. Indeed the direct calculations of the FM and AFM structures for both films give a lower energy for the AFM configuration in the case of the uncapped film and for the FM configuration in the case of the capped film.

The layer-resolved spin-polarized DOS shows an interesting thickness dependence of the spinpolarization at the Fermi level. The spin polarization increases from 30% in 1 ML to 50% in 2 ML and decreases to 30% at 3 ML coverage [1, 2]. At all thicknesses, there is a relatively large atomic magnetic moment at the sixfold-coordinated interface and the eightfold-coordinated subsurface Mn layer. For the 3 ML coverage we obtained for the lowest-energy magnetic structure the antiparallel directions of the moments of the first and third layers. The magnetic moment of the middle layer is close to zero. The FM structure of the films with 1 ML and 2 ML coverages make them interesting candidates for applications in spintronic devices.

An important requirement on the spintronic materials is a high Curie temperature. It is necessary to make the spintronic devices operative at room temperature. Below we report on the evaluation of the inter-atomic exchange parameters and the estimation of the Curie temperature. As a first step, we evaluate the Heisenberg exchange parameters by fitting the DFT energies of a number of collinear magnetic configurations with a Heisenberg Hamiltonian.

Experimentally, bulk MnSi has a low Curie temperature of $T_c = 30$ K [37]. The dependence of the magnetic transition temperature on the dimensionality of the system is a nontrivial issue since the change of the dimensionality affects the system in several ways that have an opposite effect on the magnetic transition temperature. The reduced coordination number of the magnetic atoms leads to a decreasing number of exchange interactions with neighboring atoms. This factor is expected to lead to a decreased transition temperature. On the other hand, the decreased coordination leads to less intense hybridization of the states of the magnetic atom with the environment. Narrower energy bands are the consequence of the decreased hybridization which can cause a strong increase of the atomic magnetic moments and interatomic exchange interactions. Which of these two trends prevails can be different for different systems.

According to the Mermin–Wagner theorem the presence of the magnetic anisotropy is crucial for the 2D systems to overcome the destructive consequences of the long wavelength fluctuations. The Curie temperature of the isotropic 2D ferromagnet is zero. Our estimation of MAE in the MnSi film gave the value of 0.4 meV atom^{-1}. This is comparable with the calculated anisotropy value of Fe and Co film [36]. The value of the MAE was used in the RPA calculations of the Curie temperature [3]. These calculations gave a large Curie temperatures of 241 K for a 1 ML MnSi film, and 328 K for a 2 ML MnSi film. The MFA estimations gave an even larger Curie temperature. The calculation for an unsupported 2 ML MnSi film resulted in reduced magnetic moment and the Curie temperature decreased to $T_c = 135$ K. Therefore, the interface film-substrate plays a crucial role in the formation of the magnetic properties of the film. In particular, the enhancement of the Curie temperature of the thin MnSi film due to the hybridization with Si substrate. This feature increases the potential of the films for practical applications.

Although the presence of the magnetic anisotropy is necessary to get a nonzero value of the Curie temperature the scale of the Curie temperature is much higher than the scale of MAE. The role of the magnetic anisotropy is in creating the gap in the spectrum of the long wavelength magnetic excitations. In isotropic magnets according to the Goldstone theorem this part of the excitation spectrum starts at zero energy. In a 2D system, already a small number of these excitations is sufficient to prevent a long-range magnetic ordering. The magnetic anisotropy diminishes the role of the long wavelength excitations, making strong interatomic exchange interactions, efficient in establishing the long-range ordering. We performed the calculation of the RPA Curie temperature for various values of MAE. The dependence of the Curie temperature on MAE is very strong in the region of very small MAE. In the region of realistic MAE values of the order of 0.4 meV atom^{-1} the dependence has weak logarithmic character and the value of the Curie temperature is mainly determined by the strength of the exchange interactions. The logarithmic dependence of T_c on MEA is in agreement with the rule suggested by Bruno [38].

The use of the collinear magnetic configurations for the calculation of the exchange parameters employed in our previous work [3] has a strong restriction in the evaluation of exchange interactions between distant atoms since such a calculation is connected with the use of large supercells and is very time consuming. Below we discuss a more advanced approach based on the DFT calculations for noncollinear magnetic configurations. This approach allows us to reveal interesting features of the exchange interactions not accessible with the calculations for collinear magnetic structures. We also address the important question of the limitations of the Heisenberg model in the description of the complex itinerant electron system MnSi.

The generalized translational symmetry of spiral magnetic configurations [22] allows the study of the exchange interactions between arbitrary distant atoms without performing

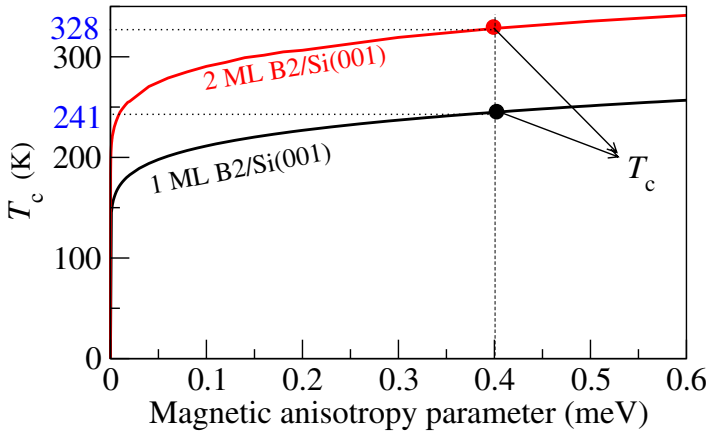

Figure 6. Curie temperature (calculated for a standard Heisenberg Hamiltonian derived from collinear magnetic configurations) versus anisotropy parameter for 1 ML (black curve) and 2 ML (red curve) coverage within RPA.

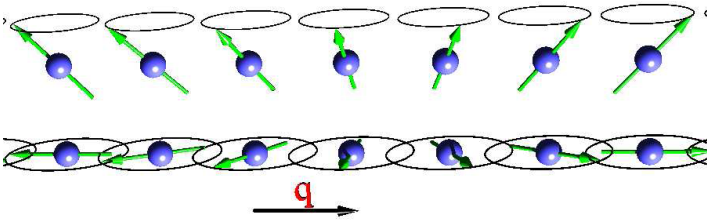

Figure 7. Two examples of the spin-spirals with the spin-rotation axis perpendicular to the spin-spiral vector **q**. The polar (cone) angles of the spirals are $\theta = \pi/2$ and $\pi/4$.

calculations for increased unit cells. The corresponding calculational scheme is usually referred to as the 'frozen magnon approach' [22]. In this method, the total energy of the spiral structures with various wave vectors (**q**) and various cone angles θ (cf figure 7) calculated within DFT are mapped on a model spin Hamiltonian.

Below we present the frozen-magnon calculations for the 1 ML MnSi film. The surface unit cell of a 1 ML film contains two inequivalent Mn atoms, which are ordered ferromagnetically. These two sublattices carry magnetic moments of $Mn_1 = 1.6$ and $Mn_2 = 2.1\ \mu_B$. The difference in the values of the moments is due to the different influence of the Si environment on the two Mn sublattices. The Mn_1 sublattice has a sixfold Si-coordination whereas the Mn_2 sublattice has a fivefold coordination.

To obtain intra-sublattice exchange parameters, we assume that the moments of each sublattice are independent adiabatic degrees of freedom. In the calculations the directions of the magnetic moments are constrained, whereas the values of the magnetic moments are relaxed within a self-consistent iterative procedure. Since we will compare the results of calculations for different magnetic configurations, it is convenient to introduce abbreviations simplifying the reference. The configuration in which the moments of the first sublattice (Mn_1) deviate from the ground-state directions whereas the moments of the second sublattice, (Mn_2) keep the ground-state directions is referred to as SP1. The configuration where the Mn_1 moments are

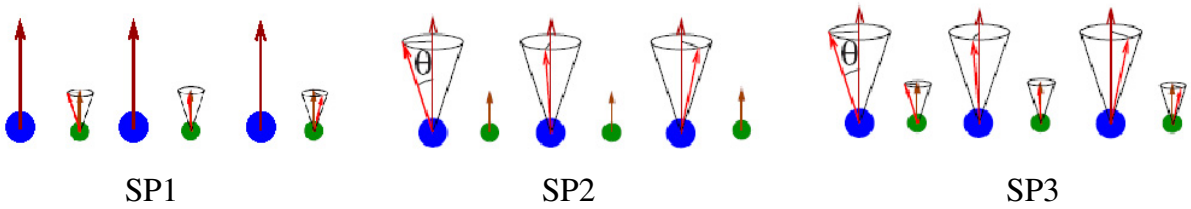

Figure 8. Schematic presentation of the SP1, SP2 and SP3 types of the frozen magnons (see text for the description).

kept parallel to the z axis and the Mn_2 moments form a spiral is called SP2. To calculate inter-sublattice exchange parameters we consider a third type of frozen magnon states. In this state, which is referred to as SP3, the moments of both sublattices deviate by the same cone angle (θ), thus forming a more complex spiral configuration. The azimuthal angles (ϕ) of the moments are determined by spiral wave vector $\mathbf{q}$. The SP1, SP2 and SP3 configurations are illustrated schematically in figure 8.

The situation is further complicated by the reduced crystallographic symmetry of the 1 ML film compared with the bulk structure. The film (shown in figure 5(c) has C_{2v} symmetry. The Mn_2 atoms continue the Si bulk lattice. They form bonds with the first layer Si substrate atoms along the x-direction. The Mn_1 atoms occupy interstitial sites of the Si-substrate lattice, and their bonds to the first layer of the substrate point along the y-direction. Hence the exchange interactions, and consequently the magnon disperison, will be different in either direction. The energy dispersion for the frozen magnons with $\theta = \pi/2$ along the high-symmetry directions in the first 2D Brillouin zone is drawn in figure 9. Unexpectedly, we obtained a very strong difference in the dispersions of SP1 and SP2 frozen magnons that reveals a strong difference in the exchange interactions within the two Mn sublattices. The form of the dispersion of the frozen magnons of the first sublattice (SP1) demonstrates the presence of strong AFM intra-sublattice interactions: the energy of the $\mathbf{q} = 0$ state (Γ point in figure 9) is higher than the energies of the states with nonzero wave vector. On the other hand, for the frozen magnon of the second sublattice the minimal energy corresponds to $\mathbf{q} = 0$, revealing the dominance of FM intra-sublattice interactions. A further increase of the frozen-magnon energies for the third type of frozen magnons shows that the leading interactions between atoms of different sublattices is also FM. This strong intersublattice FM exchange interaction stabilizes the FM structure of the film as a whole despite AFM interactions within the first sublattice.

The intra-atomic exchange parameters are obtained by means of back Fourier transformation of the frozen-magnon dispersions. Figure 10 presents the first five intra-sublattice inter-atomic exchange parameters for atoms along the x- and y-directions in the crystal lattice. We emphasize that the strong difference between the exchange interactions within the two sublattices results from the difference in the hybridization with the (nonmagnetic) Si atoms. The Mn–Si hybridization not only makes the two Mn sublattices different to each other, but also leads to the anisotropy of the exchange interactions within the sublattices. Indeed, although the Mn atoms form a square lattice, the strengths of the exchange coupling between atoms lying on the x- and y-axes are different. The anisotropy is more pronounced for the exchange interactions within the first sublattice (cf figure 10). The first nearest-neighbor intra-sublattice exchange parameter of the Mn_1 sublattice in the x-direction is positive, revealing

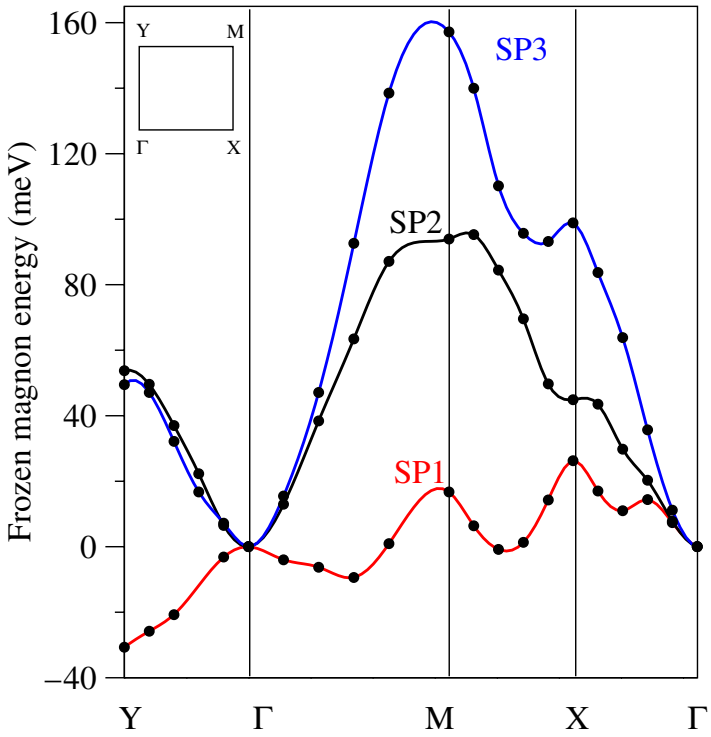

Figure 9. The energy of the frozen magnons for $\theta = \pi/2$ in high-symmetry directions of the first surface Brillouin zone.

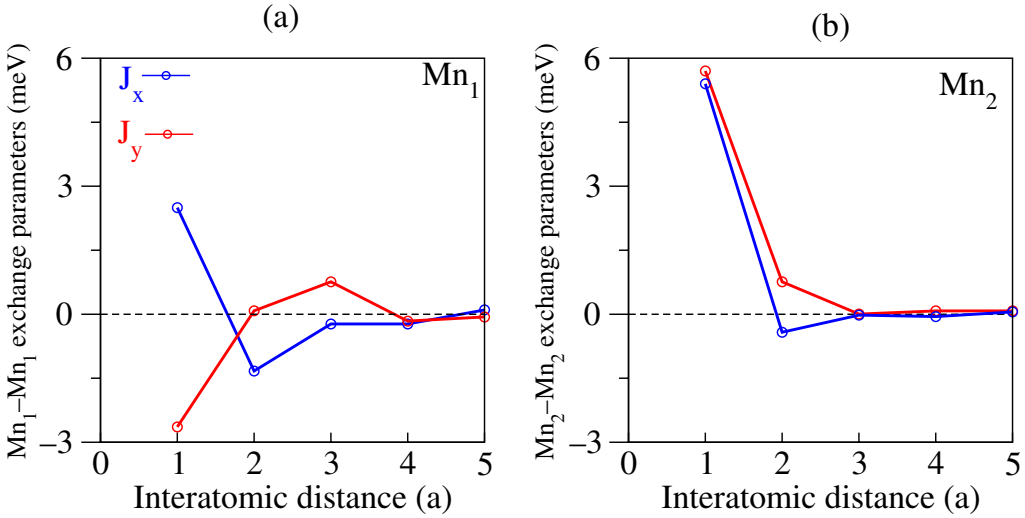

Figure 10. Intra-sublattice exchange parameters for atoms along the x-(blue curve) and y-(red curve) directions for Mn_1 (a) and Mn_2 (b) sublattices.

FM coupling, whereas the corresponding exchange parameter in the y-direction is negative, revealing AFM coupling.

The procedure to obtain the inter-sublattice exchange parameters is more complicated. The intra-sublattice contributions must be subtracted from the total dispersion before performing

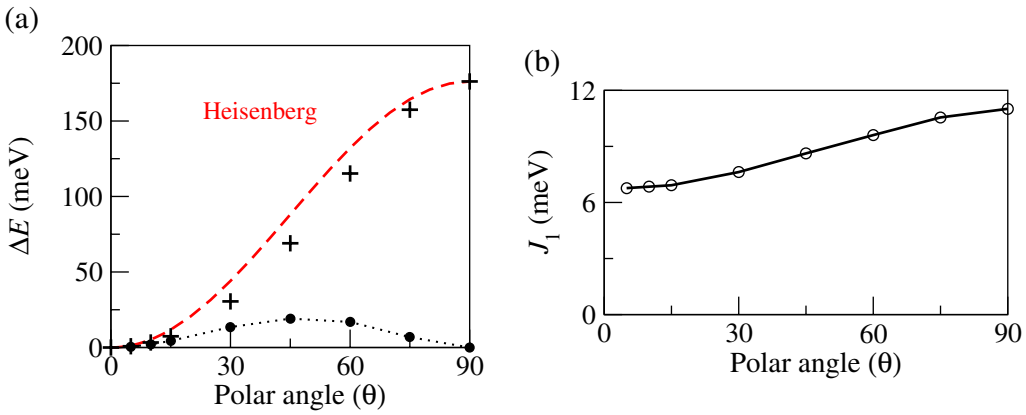

Figure 11. (a) Calculated energies of the relative rotation of the moments of two Mn sublattices by angle θ(+). The dashed curve represents a Heisenberg-type dependence. The dotted curve gives the difference between the calculated and Heisenberg-type dependencies. (b) The Heisenberg parameter of the exchange interaction between sublattices as a function of angle θ.

the back Fourier transformation. The frozen-magnon technique for the determination of the exchange interactions for complex crystal structures has been recently discussed in detail by Sandratskii *et al* [27]. Here, we do not perform a full analysis of the inter-sublattice exchange parameters. By means of the analysis of the **q** dependence of the SP3 frozen-magnon dispersion for the $\Gamma \rightarrow$ M interval we came to the conclusion that the nearest-neighbor intersublattice exchange interaction is much stronger than the inter-sublattice exchange interactions between more distant atoms. The estimated value of the nearest-neighbor interaction is 11 meV.

Next, we describe several calculations aiming to verify the validity of the Heisenberg model (equation (10)) in the description of the MnSi films. We first calculate the energy of the relative deviation of the moments of two Mn sublattices by an angle 2θ. According to the Heisenberg Hamiltonian the θ-dependence of this energy must be exactly proportional to $1 - \cos 2\theta$. Therefore, the deviation from this functional form reveals the restriction of the Heisenberg model. In these calculations, we use the magnetic force theorem [17, 39]. According to this theorem, the difference of the total energies of two magnetic states can be approximated by the difference of the corresponding band energies. The self-consistent calculation is carried out for only one of the two states. The potentials thus obtained are used to evaluate the band energy of the second magnetic state. The use of the force theorem greatly reduces the calculational demands.

In figure 11(a), we compare the energy as a function of θ with the corresponding Heisenberg-type function. The comparison shows the deviation of the calculated energies from a simple cosine-like function. These deviations are symmetric with respect to the angle $\theta = \pi/4$ (cf dotted curve in figure 11(a)).

The ratio of the Heisenberg energy to $1 - \cos 2\theta$ should be independent of θ. However, a similar ratio for the calculated curve shows strong θ-dependence (figure 11(b)) varying from 6.8 meV at small θ to 11.0 meV for $\theta = \pi/2$. The strong θ-dependence of the ratio indicates the limited validity of the Heisenberg model in the account of transversal magnetic fluctuations. The deviation from the Heisenberg model can be treated as a θ-dependence of the exchange

parameters. A rigorous statistical-mechanics model must take into account the full complex character of the energetics of the system. Such statistical-mechanics calculations are a nontrivial problem that needs separate consideration and will not be addressed in this paper.

We will simplify the problem and put the question in the form: which value of θ should be chosen that the exchange parameters give the best estimation of the Curie temperature of the system within the Heisenberg model? The answer to this question depends on the typical angles between atomic moments when the system is close to the Curie point, and is directly related to the strength of the short-range magnetic order (SRMO) at this temperature. Note that both experimental and theoretical studies do not provide unique answer on the temperature dependence of the SRMO. Opinions deviate cardinally even in the case of elementary $3d$-ferromagnets [41, 42].

The assumption of strong SRMO corresponds to low-θ values of the exchange interaction. On the other hand, if the SRMO is negligible, the average angle between different moments is $\theta = \pi/2$, and values of the exchange interaction should be taken from the large-θ calculations. The consequences of this choice for the predicted Curie temperature are obvious already on the level of a mean-field estimation: assuming nearest-neighbor exchange interactions and using low-θ values of the parameters gives 230 K, whereas the large-θ parameters yield 380 K. As the strength of the SRMO in MnSi is yet unknown, an optimal choice of the exchange parameters needs further studies.

Moreover, the calculation of the frozen-magnon energies as a function of the wave vector can be used to study the restrictions of the Heisenberg model. We performed the calculation of the frozen-magnon dispersions for three values of the θ angle: $\pi/4$, $\pi/3$ and $\pi/2$. The calculations for each of these angles is sufficient to evaluate the Heisenberg exchange parameters. The difference between exchange parameters obtained for different θ reveals the restrictions of the Heisenberg model in the description of the given system. We visualize these restrictions by using the exchange parameters obtained for $\theta = \pi/2$ to describe the frozen-magnon dispersion for $\theta = \pi/3$ and $\theta = \pi/4$. In figure 12, we draw the frozen-magnon energies as a function of the wave vector $\mathbf{q}$ for the [110]-direction of the 2D reciprocal space. We find a strong deviation of the results obtained with the use of the exchange parameters from $\theta = \pi/2$ calculations from the values obtained in direct calculations for different θ. This difference visualizes again the limitations of the Heisenberg model where the exchange parameters obtained for one θ must reproduce exactly the energies obtained for another θ.

To overcome the limitations of the Heisenberg model in the description of the energetics of the system we have to include into the model Hamiltonian higher order terms such as biquadratic and three-spin interactions.

$$H = -\sum_{i,j,\mu,\nu} J_{ij}^{\mu\nu} \mathbf{e}_{i\mu} \cdot \mathbf{e}_{j\nu} + \sum_{i,j,\mu,\nu} k_{ij}^{\mu\nu} (\mathbf{e}_{i\mu} \cdot \mathbf{e}_{j\nu})^2 \tag{10}$$

In figure 13, we compare the fitting obtained with the standard Heisenberg Hamiltonian and the fitting with Heisenberg plus biquadratic terms. The calculations show that the inclusion of the biquadratic term is sufficient to reach very good descriptions of the frozen magnon energies obtained for different θ values (figure 13).

A characteristic feature of the itinerant-electron systems is the possibility of longitudinal fluctuations of the atomic moments. The variation of the magnitude of the atomic moments for a given magnetic configuration is neglected in the Heisenberg model. To study the energetics of longitudinal fluctuations we use the fixed-spin-moment method.

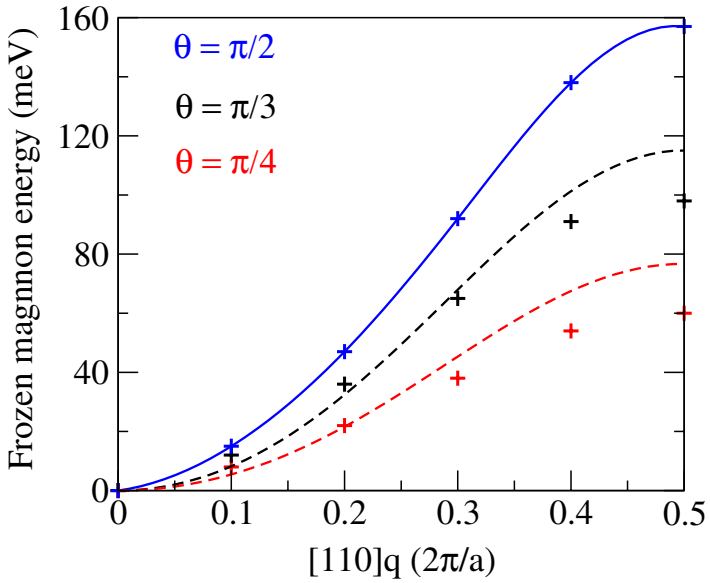

Figure 12. Frozen magnon energy as a function of spin wave vector for (110) direction of the reciprocal space. The calculations are performed for three values of angle $\theta = \pi/4, \pi/3$ and $\pi/2$. The calculated value are given by sign (+). The curves show the corresponding dependencies obtained with Heisenberg Hamiltonian with exchange parameters obtained by the Fourier transform of the $\theta = \pi/2$ data points. These calculations are performed for SP3 type of magnons.

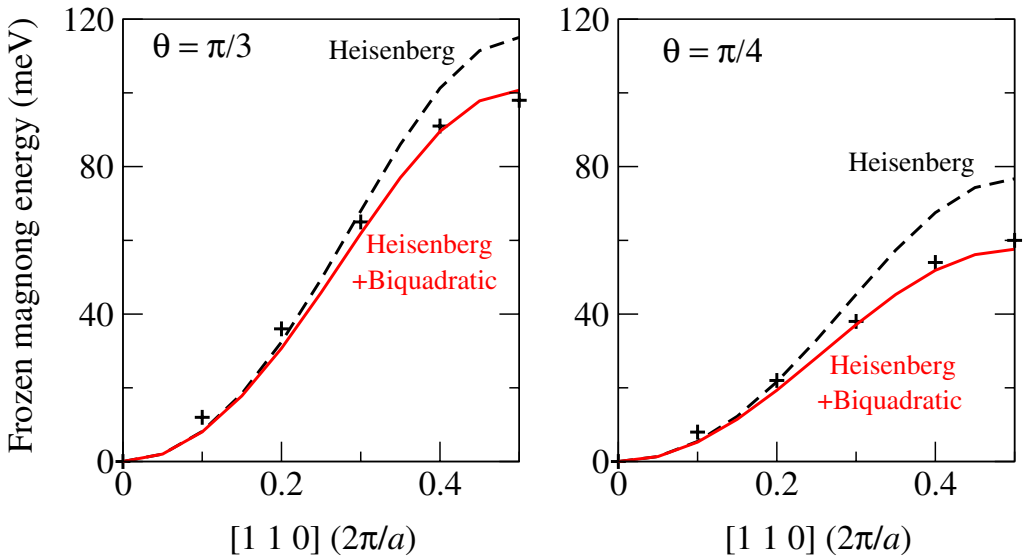

Figure 13. The role of the biquadratic exchange interaction. Solid lines show dispersion obtained with the Heisenberg plus biquadratic terms. Dashed lines show the dispersion obtained with the standard Heisenberg Hamiltonian.

We consider the FM ground state and impose a constraint on the value of the spin moment of the atoms of the first sublattice. This constraint corresponds to an effective magnetic field acting on the atoms of the first sublattice only. The value of the effective field for a given value of

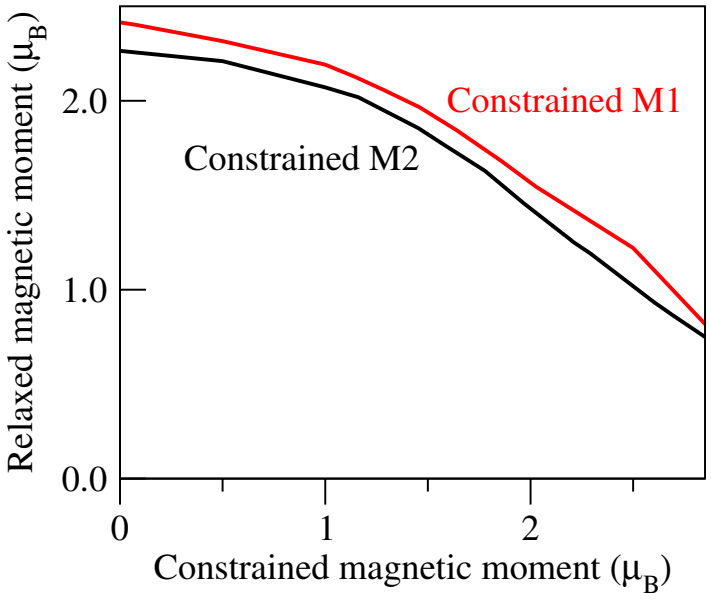

Figure 14. Variation of magnetic moment of the Mn sublattice as a function of the constrained moment of the other sublattice. The red (black) curve shows the moments of sublattice Mn_2 (Mn_1), whereas the moment of the other sublattice is constrained.

the moment is obtained within a self-consistent procedure. Although the field acts on the atoms of one sublattice only the calculations show that the value of the moment of the second sublattice also vary. This variation is the result of the inter-atomic hybridization. Rather unexpectedly, the increase of the constrained moment leads to the decrease of the moment of the other sublattice. The induced variation is very strong, about 50% of the variation of the constrained moment (see figure 14). Therefore, the changes of the moments of two sublattices partly compensate each other. A similar type of relation between induced and inducing magnetic moments was recently obtained in calculations of the half-metallic compound NiMnSb [43].

The effective magnetic field versus the constrained value of the magnetic moment is shown in figure 15(a). The ground-state value of the moment corresponds to vanishing constraining field. The total energy as a function of magnetic moment can be obtained by integration of the constraining field as a function of the moment. Figure 15(b) presents the total energy as a function of constrained moment of the Mn_1 or Mn_2 atom. These curves give the characteristic energies of the excitations of the system connected with the variation of the values of the atomic moments. The energy as a function of the moment has the shape of an asymmetric parabola with a minimum at the ground-state value of the moment (m_0). A fit of the energy curve around the minimum with the function $y = a(x - m_0)^2$ gives the coefficient $a = 0.09\,(0.10)\,\text{eV}\,\mu_B^{-2}$ for the case of the 1st (2nd) constrained sublattice. The contribution of the longitudinal fluctuations to thermodynamic quantities at a given temperature can be estimated from the interval of the values of the magnetic moment corresponding to an energy variation of the order of $k_B T$. For a flatter curve (smaller a), the contribution of the longitudinal fluctuations increases.

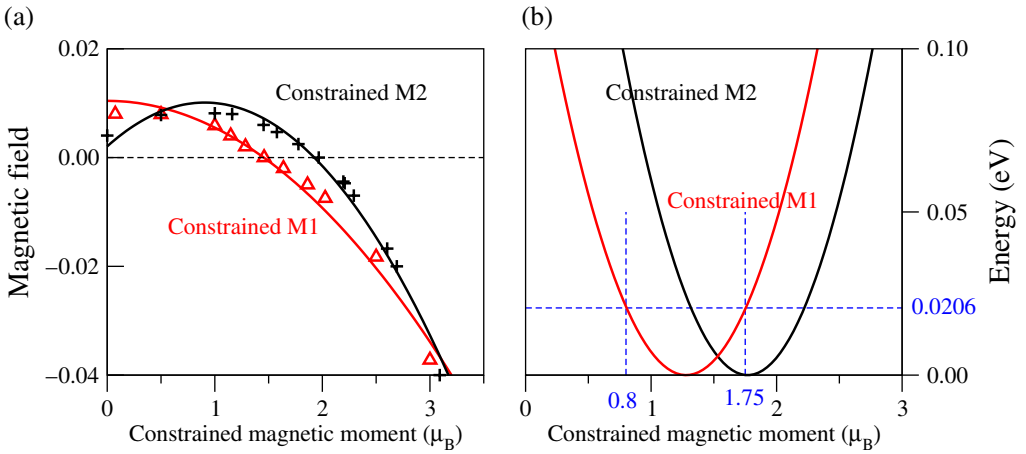

Figure 15. (a) Constraining magnetic field versus the constrained value of the magnetic moment. The red (black) curve shows the dependence obtained with constrained moment of the first (second) sublattice. (b) The total energy as a function of constrained magnetic moment of sublattices. The broken horizontal line refers to the energy corresponding to the Curie temperature of 241 K.

The contribution of the longitudinal fluctuations to thermal averages is negligibly small if the characteristic energies of the transversal fluctuations described by the Heisenberg Hamiltonian are much smaller than the characteristic energies of the variation of the value of the atomic moments. To estimate the importance of the longitudinal fluctuations, we consider the energy corresponding to the estimated Curie temperature of the 1 ML-film (241 K). In energy units, this temperature gives $E_{\mathrm{M}} = 20.6\,\mathrm{meV}$. Taking this value as a maximal excitation energy for the variation of the value of the moment, we obtain the following intervals of the variation of the moments: $0.80\mu_{\mathrm{B}} < M_1 < 1.75\mu_{\mathrm{B}}$ and $1.30\mu_{\mathrm{B}} < M_2 < 2.25\mu_{\mathrm{B}}$ for the Mn_1 and Mn_2 moments, respectively (see figure 15(b), blue lines). Therefore, the contribution of longitudinal spin fluctuations to the thermodynamics of the MnSi films is expected to be considerable and should be taken into the account.

On the basis of the above considerations the energy of an arbitrary magnetic configuration contains contributions coming from the change of the relative directions of the atomic moments as well as from the change of the values of the atomic moments. The first contribution is determined by the interatomic exchange parameters and the second contribution by the longitudinal stiffness of the moments. In general, these contributions are not independent of each other.

4. Conclusion

Our calculations show that for a adsorption of single Mn in the Si(001), the incorporation of Mn into the subsurface interstitial sites is energetically favored and associated with a small activation barrier. This barrier is lower than on-surface diffusion barriers. Once Mn atoms have reached the subsurface site, their mobility is drastically reduced since further diffusion into the bulk as well as reverse diffusion to the surface is energetically rather costly. Despite Si(001) is structurally an anisotropic surface, diffusion of Mn is almost isotropic on the surface in both the direction parallel and perpendicular to the dimer rows.

Our calculations indicate the possibility of formation of multilayered MnSi films that have a B2 crystal structure (sandwiches of Mn and Si layers). In these sandwiches, the Mn atoms near the surface and interface have larger magnetic moments, which are coupled ferromagnetically within the layers. The layer-resolved electronic DOS indicates a considerable degree of spin polarization at the Fermi level, up to 30 and 50% for one and two MnSi layers, respectively.

We study exchange interactions between Mn atoms and show that the decreasing number of coordination of the Mn atoms in the MnSi film leads to an increase of both the magnetic moments and Heisenberg exchange parameters. In the evaluation of the Curie temperature, we take into account the magnetic anisotropy. For the calculated MAE of 0.4 meV per Mn atom, the Curie temperature assumes the values of 241 and 328 K for one and two monolayer MnSi films, respectively. Since the Curie temperatures are rather high, MnSi layers grown on Si(001) are promising components for applications in spintronics devices.

Finally, we demonstrate that dispersion of magnetic excitations in MnSi films deviate strongly from standard Heisenberg behavior. The study of the temperature dependence of the magnetic properties of the films that goes beyond the Heisenberg model could be a topic of future work.

Acknowledgments

We thank Matthias Scheffler for initiating the project and valuable discussions. In the initial stages, this work benefited from discussions with Hua Wu on FM MnSi films.

References

[1] Wu H, Hortamani M, Kratzer P and Scheffler M 2004 *Phys. Rev. Lett.* **92** 237202
[2] Hortamani M, Wu H, Kratzer P and Scheffler M 2006 *Phys. Rev.* B **74** 205305
[3] Hortamani M, Sandratskii M L, Kratzer P, Mertig I and Scheffler M 2008 *Phys. Rev.* B **78** 104402
[4] Kratzer P, Hashemifar J, Wu H, Hortamani M and Scheffler M 2007 *J. Appl. Phys.* **101** 081725
[5] Dalpian G M, da Silva A J R and Fazzio A 2003 *Phys. Rev.* B **68** 113310
[6] Dalpian G M, da Silva A J R and Fazzio A 2004 *Surf. Sci.* **688** 566
[7] da Silva A J R, Fazzio A and Antonelli A 2004 *Phys. Rev.* B **70** 193205
[8] Liu Q H *et al* 2008 *Phys. Rev.* B **77** 245211
[9] Krause M, Stollenwerk A, Reed J, LaBella V, Hortamani M, Kratzer P and Scheffler M 2007 *Phys. Rev.* B **75** 205326
[10] Liu H and Reinke P 2008 *Surf. Sci.* **602** 986
[11] Sjöstedt E, Nordström L and Singh D J 2000 *Solid Stat. Commun.* **114** 15
[12] Blaha P, Schwarz K, Madsen G K H, Kvasnicka D and Luitz J 2001 WIEN2k, *an Augmented Plane Wave + Local Orbitals Program for Calculating Crystal Properties* ed K Schwarz (Austria: Technische Universität Wien)
[13] Perdew J P, Burke K and Ernzerhof M 1996 *Phys. Rev. Lett.* **77** 3865
[14] Eder M, Hafner J and Moroni E G 2000 *Phys. Rev.* B **61** 11492
[15] Hortamani M 2006 Theory of adsorption, diffusion and spin polarization of Mn on Si(001) and Si(111) substrates *PhD Thesis* Freie Universität, Berlin
[16] Wu H, Kratzer P and Scheffler M 2005 *Phys. Rev.* B **72** 144425
[17] Liechtenstein A I, Katsnelson M I, Antropov V P and Gubanov V A 1987 *J. Magn. Magn. Mater.* **67** 65
[18] Stampfl C *et al* 1999 *Phys. Rev. Lett.* **83** 2996
[19] Sinai Y G 1982 *Theory of Phase Transitions: Rigorous Results* (Oxford: Pergamon)

[20] Mermin N D and Wagner H 1966 *Phys. Rev. Lett.* **17** 1133
[21] Anderson P W 1963 *Solid State Physics* vol 14 ed F Seitz and D Turnbull pp 99–214
[22] Sasioglu E, Sandratskii L and Bruno P 2004 *Phys. Rev.* B **70** 024427
Sasioglu E, Sandratskii L and Bruno P 2005 *Phys. Rev.* B **71** 214412
[23] Sasioglu E, Sandratskii L, Bruno P and Galanakis I 2005 *Phys. Rev.* B **72** 184415
[24] Rusz J, Turek I and Divis M 2005 *Phys. Rev.* B **71** 174408
[25] Williams A R, Kübler J and Gelatt C D 1979 *Phys. Rev.* B **19** 6094
[26] Sandratskii L M 1998 *Adv. Phys.* **47** 91
[27] Sandratskii L, Singer R and Sasioglu E 2007 *Phys. Rev.* B **76** 184406
[28] Hortamani M, Sandratskii L M and Mertig I 2009 *J. Magn. Magn. Mater.* in press
[29] Dederichs P H, Blügel S, Zeller R and Akai H 1984 *Phy. Rev. Lett.* **53** 2512
[30] Beeler F, Andersen O K and Scheffler M 1990 *Phys. Rev.* B **41** 1603
[31] Gilles D, Bergholz W and Schröter W 1986 *J. Appl. Phys.* **59** 3590
[32] Lippitz H, Paggel J J and Fumagalli P 2005 *Surf. Sci.* **575** 307
[33] von Känel H, Schwarz C, Goncalves-Conto S and Müller E 1995 *Phys. Rev. Lett.* **74** 1163
[34] Hobbs D and Hafner J 2001 *J. Phys.: Condens. Matter* **13** L681
[35] Stoner E 1936 *Proc. R Soc.* A **154** 656
[36] Pajda M, Kudrnovsky J, Turek I, Drchal V and Bruno P 2000 *Phys. Rev. Lett.* **85** 5424
[37] Pfleiderer C 2001 *J. Magn. Magn. Mater.* **226–230** 23
[38] Bruno P 1992 *Mater. Res. Soc. Symp. Proc.* **321** 299
[39] Mackintosh A K and Andersen O K 1980 *Solid State Physics* vol 35 ed H Ehrenreich, F Seitz and D Turnbull (New York: Academic)
[40] Liechtenstein A I, Katsnelson M I, Antropov V P and Gubanov V A 1987 *J. Magn. Magn. Mater.* **67** 65
[41] Antropov V 2005 *Phys. Rev.* B **72** 140406
[42] Ruban A V, Khmelevskyi S, Mohn P and Johansson B 2007 *Phys. Rev.* B **75** 054402
[43] Sandratskii L M 2008 *Phys. Rev.* B **78** 094425